International Journal of Computing and Digital Systems
ISSN (2210-142X)
Int. J. Com. Dig. Sys. 12, No.1 (Aug-2022)

https://dx.doi.org/10.12785/ijcds/120156

New Approach for Reducing Impact of Sand Storm and Subsequent Deposition on Solar Panel in Desert Area

Sudip Das[1], Pritam Kumar Gayen[2] and Debamoy Datta[3]

[1]*Electrical Engineering Department, JIS College of Engineering, Kalyani, India*
[2]*Electrical Engineering Department, Kalyani Government Engineering College, Kalyani, India*
[3]*Electrical Engineering Department, JIS College of Engineering, Kalyani, India*

Received 14 Jan. 2022, Revised 16 Jul. 2022, Accepted 23 Jul. 2022, Published 6 Aug. 2022

Abstract: In desert areas, solar panels are extensively used to convert solar energy into electrical energy as a potential source of the free energy. The solar panel in the remote locations suffers from frequent problem due to sand storm erosion effect. In effect, performance of the solar panel in desert areas is degraded. Previous studies explained how to use self-cleaning coats or active method that can reduce the impact of the sand particles but cannot avoid the attack forces of the sand storm. Thus, the work of this paper proposes a novel strategy to reduce erosion effect with the help of a motor-drive of tracker system. The erosion prevention strategy minimizes the attacking force of moving sand particles on the front surface of a panel during a sand storm. In this regard, the impact is virtually analyzed to demonstrate the effectiveness of the proposed strategy under the sand storm. In the study, a procedure for determining optimum tilt angle of solar panel is described. In the tilting condition, striking velocity on the front-face of solar panel is significantly reduced. Here, the minimum value of air velocity on the solar panel's surface is observed. It causes less erosion on the glass cover. Thus, the possibility of degradation rate of panels in desert areas is appreciably reduced and hence, the performance of the solar panels is improved as per the analysis of this paper. In addition, subsequent sand removal activity is done through jerking methodology by geared electric drive system after the storm. Thus, sand deposition on the solar panel due to storm is greatly avoided.

Keywords: Solar panel, dust storms, erosion, computational fluid dynamics, nanoCAD

1. Introduction and Overview

Solar panels and their associated technologies have been subjected to intense research in the present decade. The massive usages of the solar panel in desert areas are noticed due to favorable environment. The deep investigations on degraded performance of solar panel in the remote areas are found in the works [1], [2]. The problem is more severe in deserts due to significant presence of sand particles in air, where dust storms occur frequently [3] and as a result, degradation of solar panel's life and performance is more rapid in those areas as compared to other areas [4]. The degradation of solar panel's life and performance occurs due to sandstorm erosion process in deserts. Also, the subsequent sand deposition after storm reduces its performance. The process of delivering the dust to the surface of the PV module is mainly due to wind, known as the aeolian process. The uptake of the airborne particles from the ground depends on the near-surface dynamics. In a paper by Albugami, Palmer, and others, the frequency of dust storms in Saudi Arabia is discussed, wherein a year on an average more than 100 dust storms occurs and, in every month, a minimum of 3 to 5 dust storms occur [5]. In this case, the storm would degrade the panels even more quickly as compared to the ordinary conditions. Although a huge potential exists for the establishment of solar panels in desert areas, it is hindered by the presence of such dust storms. After sand storm, there is accumulation of sand over the panel, which is to be cleaned for improving its performance.

A novel strategy is suggested to reduce sandstorm erosion by using motor-drive of solar-tracking system (it is commonly available in most of the solar plant in desert areas). Here, solar tracking activity is not hampered as it is normally not used during sand storm. If sand storm is detected, the motor-drive system changes orientation of solar panel so that minimum erosion of its glass cover occurs. In this respect, an optimum angle is proposed. Here, a procedure for the determination of optimum tilt angle is virtually done to minimize the impact of blowing wind on solar panels and their supporting structure. The erosion is

E-mail address: sudipdas1380@gmail.com, pkgtar@gmail.com, datta.debamoy@gmail.com

quantified to justify its significant reduction during a sand storm.

The novel methodology also performs dust cleaning activity after the storm. It uses before mentioned motor-drive for the cleaning purpose. Here, rapid clockwise and anti-clockwise angular movement of solar panel up to some angle with the help of motor-drive system is suggested, which has similarity in the working of washing machine. However, it helps to remove loose sand accumulated over the panel. The proposed method does not incur extra cost as it shares the motor-drive of tracking system i.e., it is cost-effective solution also.

2. Background study and motivation

A. *Background study*

Here, various non-daily cleaning methods (as per necessity), and sandstorm erosion phenomena as reported in published literatures are discussed. In a paper proposed by Kumar, Sudhakar, and others, the concept of an innovative dust cleaning robot for the solar panels on building structures had been reported [6]. In another paper by Wable and Ganiger, energy-efficient cleaning method for the solar panels had been developed by employing a nylon brush in the form of a roller, which is made from soft bristles [7]. Here, the brush rotates at high speed for throwing the dust out from the panel. In another work by Naik and others, the cleaning unit moves on the solar panel in an oscillatory motion, which is tracing over the entire panel surface [8]. The cylindrical brush that is mounted on the cleaning unit rotates in the clockwise direction. Along the entire path, it forces the dust to move in the direction of the motion of the cleaning unit and finally blows it away at the edge of the panel. In a thesis proposed by Matt, Burke, and others, a special kind of apparatus is developed that utilizes a brush cleaning system that cleans on a set of cleaning cycles [9] . The device used a combination of gear trains with 48 pitch Delrin gears and 12V rated DC motors to spin both a 5.00 ft long, 0.25-inch diameter vacuum brush shaft and drive two sets of two wheels. The power source for the drive train is a 12V deep cycle type lead-acid battery. In another paper proposed by Rathode, Bhavsar, and others, a wiper-based cleaning system is developed [10]. Here, water along with a car-based wiping system had been used. In a paper, the interaction between dust and solar panel surface is evaluated in connection with soiling problem [11] . The effect of high-velocity sand and dust on PV panels/reflectors is discussed in several literatures [12][13][14][15].

B. *Motivation and Outcomes*

All conventional dust removal methods need extra arrangements and thus, these incur extra expenditure. The performance of these methods under high accumulation of sand over solar panel just after sand storm may not be effective. Therefore, a cost-effective post-storm accumulated dust removal technique is proposed in this paper. Here, substantial driving force by tracker motor is created over solar panel through jerking process like in a washing machine. Thus, more effective way for removing sand after storm is suggested in this work.

During sand storm, inclination of solar panel to minimize erosion effect on its front face by blowing sand is not analyzed in published articles to the best of authors knowledge. In this context, authors investigate the contact of blowing air with the glass surface of solar panel through computational fluid dynamics (CFD) software. Also, the lift and drag forces by the blowing wind under the storm are observed to find out minimum stress on the solar panel. From the observations of studies on erosion and stress effects, optimum inclination of the panel is proposed in the work.

The above said jerking process and inclination of solar module with help of tracker drive is experimentally tested.

In the suggested method, detections of initiation and subsequent stopping of the storm are needed to drive the motor for reorientation of panel and dust removal purpose respectively. This is done by monitoring change in pressure. In this regard, validation of proposed control logic is also verified through PSIM software.

Section 3 describes proposed methodology. Analytical studies, results and performance evaluation are presented in section 4. Section 5 states conclusions. References are given at the end of this paper.

3. Proposed Methodology

The stepper motor-based tracking arrangement is given in the block diagram of Fig. 1.

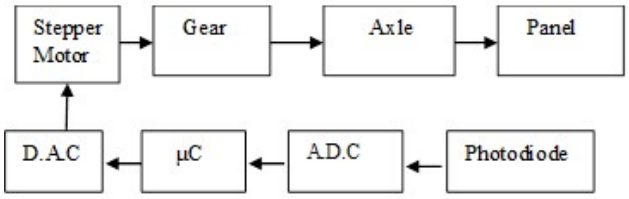

Figure 1. Block diagram of tracking arrangement.

The motor-drive can be used for both tracking and sandstorm erosion prevention purposes. Thus, no substantial extra cost is involved in serving erosion and subsequent soiling prevention purposes due to sand storm. Here, the motor-drive used in tracking arrangement is utilized for making reorientation of the solar panel during the sand storm to minimize the velocity impact on the panel. Then, accumulated dust due to storm is removed by the drive system. The proposed schemes are described in detail as follows:

A. *Proposed Methodology for Reducing Erosion during Sand Storm*

The system, which is shown in Fig. 2, predicts the weather condition using the pressure variations for a time

interval [16]. If a storm is detected, then the panel is rotated in such a manner that the front glass of panel faces the ground. In such a process, the dusts fall off due to gravity. Here, some particles may stick due to cohesion. This system is normally used to reduce direct contact with sand particles during the storm. But the proposed strategy further investigates to find the other orientation to further reduce the impact of blowing sand particles on the glass surface of panel. At first, detection of storm and its direction are essential in this regard. Then, the optimum orientation of the solar panel is suggested. The process steps are explained as follows:

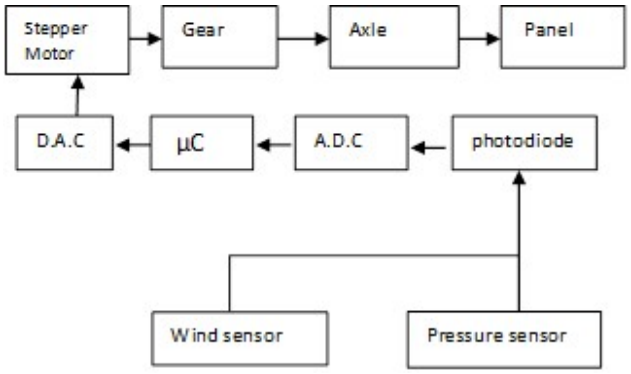

Figure 2. Block diagram of the proposed method for erosion reduction purposes during a sand storm.

At first, the detection of storm is discussed. A steadily falling pressure indicates occurrence of a storm. This meteorological prediction method can give accurate predictions in short duration. Here, the score 'M' is calculated in below, which provides a quantitative indication of occurrence of storm,

$$M = ((P_2 - P_1))/((t_2 - t_1)) \quad (1)$$

The expression in (1) is the slope calculated over a period of time. If the slope is less than a critical negative value, then the storm is approaching else the weather would remain fine. If the pressure is decreasing by 1mb/hour, then a storm is approaching. In the storm detection scheme, four wind sensors are used in four principal directions, which are used to measure wind speed and direction of wind flow during the storm. The wind sensors-based logic is tested using PSIM software, which will be given in the result section. Next, steps of orientation of panel are discussed. In Fig. 3, step 1 starts if the storm is detected. In step 1, the panel is rotated such that the front surface of the panel faces the ground. In step 2, the panel is further tilted at an optimum angle by either clockwise or anti-clockwise rotation of tracking motor on the basis of detected wind direction as shown in Fig. 3. The optimum tilting angle is required to be calculated so that net striking air velocity on front face is minimized (reduction of erosion). Also, stress on the mounting structure needs to be simultaneously assessed to assure the structure safety. It improves the reliability of the panel and its mounting structure. Here, the optimum angle is found as -31 degree as marked in Fig. 3. The novel procedure of finding the optimum tilt angle will be illustrated in the result section (section 4).

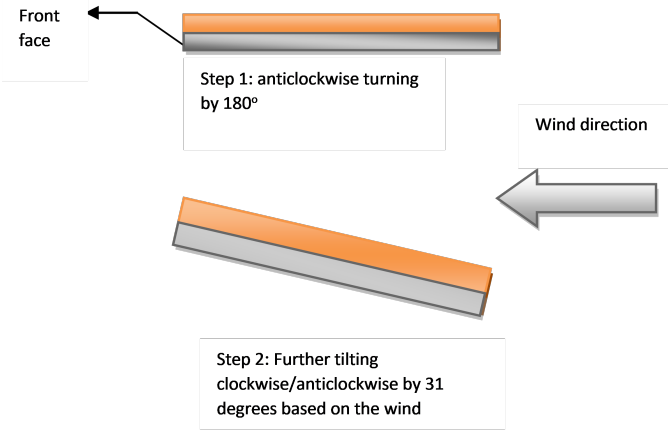

Figure 3. Steps for tilting at optimum angle (-31 degree)..

B. Proposed Methodology for Removal of Accumulated Sand after Storm

As shown in Fig. 4(b), a small clockwise, as well as anti-clockwise rotation, is given to the axle mounted panel (Fig. 4(a)) by a gear drive mechanism (employing the motor-drive used in tracking arrangement as shown in Fig. 1) alternately (angular movement in some degree). This overcomes the adhesive force between the panel and accumulated dust over it. This procedure is repeated just after storm. This process is similar to the operation of washing machine for cleaning purpose. Here, a sharp transition of the rotational movement is required so that large proportion of dust deposited over panel is removed. The rapid transition of gear-based motor-drive system in connection with dust removal process is described with help of mathematical analysis as follows: The torque balance equation is represented as,

$$T_e = Tmshaft + Taxle + Tdamp\_mshaft + Tdamp\_axle) \quad (2)$$

In (2) Te is the torque developed by the motor, $Tmshaft$ is the torque required to overcome the inertia of the motor shaft. $Taxle$ is the torque required to turn the axle. $Tdamp\_mshaft$ is the damping torque due to the air on the motor shaft. T_damp_axle is the damping torque on the axle due to air. There is a gearbox between motor shaft and axle, whose turns ratio can be adjusted by the clutch.

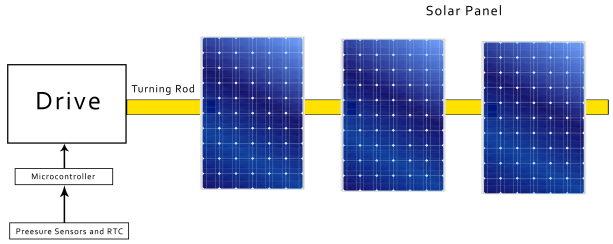

(a) Axle-mounted solar panels driven by motor-drive

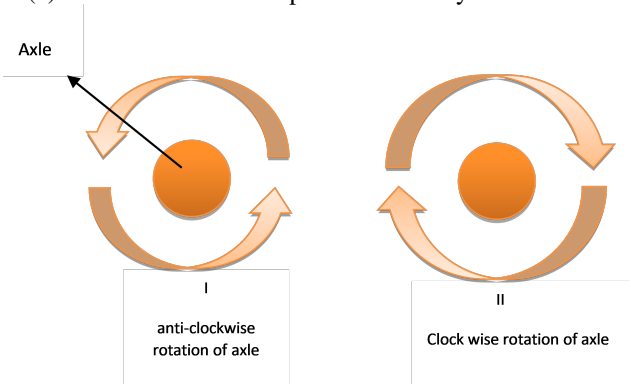

(b) Clockwise and anti-clockwise rotation of driving axle

Figure 4. Schematic diagrams.

Now, (3) is mathematically expressed due to the presence of gears,

$$\Theta_a xle/\Theta_m shaft = N/1 \tag{3}$$

In (3), N is the gear ratio, From Stoke's law, it is written as,

$$Fdamp = 6\pi\eta Rv \tag{4}$$

Where v is the linear velocity, 'r' is the radius of the axle, and η is the coefficient of viscosity of air, in this case, multiplying the (4) on both sides by 'r' and get,

$$Tdamp = 6\pi\eta R\omega \tag{5}$$

In (5) 'ω = rv' is the angular velocity of the axle and $Tdamp$ is the damping torque. In case of axle, it becomes $Tdampaxel$ and it becomes $Tdampmshaft$ at motor shaft. The presence of gear causes different angular velocity at motor shaft from that of axle. By putting (5) in (2) for axle and motor shaft the mathematical relationship is written as,

$$T(t) = Jmshaftd^2\Theta mshaft/dt^2 + Jaxle$$

$$d^2\Theta axle/dt^2 + 6\Pi\eta Rd\Theta mshaft/dt + 6\Pi\eta Rd\Theta axle/dt(6)$$

(6) By using the relationship between and for gears in (3), the (6) becomes,

$$\Theta axle(s)/T(s) =$$

$$1/\ [(\text{Jmshaft}/\ \text{N}\ s^2 + Jaxles^2)6\Pi\eta R1/Ns + 6\Pi\eta Rs](7)$$

The (7) expresses the transfer function of the system with torque as the input and angular position as the output. Now, the settling time is to be reduced to have a sharp transition. Thus, the pole of the transfer function needs to be changed. Equating the characteristic polynomial of (7) to zero, the roots are found as s=0 and,

$$s = -6\Pi\eta R(1/N + 1)/(Jmshaft/N + Jaxle) \tag{8}$$

In a White paper by Mitsubishi electric, a detailed discussion about the change in the resonant frequency with change in gear ratio is discussed [17]. For the case in this paper, this fact can help to reduce the settling time. Here, the elastic fatigue has neglected for simplification as small angular displacements are considered. Now, the motor shaft's moment of inertia and the axle's moment of inertia is related to each other as:

$$Jaxle = Jmshaft/N^2 \tag{9}$$

Substituting of $Jmshaft$ in (9) to (8), the pole value becomes,

$$\text{s=-}6\Pi\eta R(1/N + 1)/((N + 1)Jaxle)$$

Thus, position of the pole of this system can be changed by changing the gear turns ratio. The transfer functions in (7), after simplification, is expressed as,

$$G(s) = 1/[(N + 1)Jaxle]s^2 + 6\Pi\eta R(1/N + 1)s \tag{10}$$

The (10) is general transfer function considering applied torque as the input and the angular displacement as the output. Using simplified assumptions, Kg.m2, and by choosing the radius of the axle such that , the above transfer function in (10) becomes,

$$G(s) = N/(N^2 + N)s^2 + (N + 1)s \tag{11}$$

By incorporating a power transistor amplifier at the input of the motor, armature current in the armature winding is increased by times. The torque developed by the stepper motor is proportional to the armature current i.e., T α Ia If Ia becomes βIa , then the torque would increase by β times to that of without amplifier case. Hence, the gain is increased by the factor of β .

$$G(s) = \beta N/(N^2 + N)s^2 + (N + 1)s \tag{12}$$

In the transfer function in (13), input quantity is applied torque and the output is the angular displacement as stated before. A power electronic amplifier has been used in the power circuit to drive the motor. This amplifier is acting as a proportional controller. The simulation considers a fixed value of proportional gain. In (13), the fast settling of angular displacement aids removal of substantial proportion of dust particles from the panel. It decides rate of change of angular displacement of the axle holding the panels. The impulse response is considered for the stepper motor. Here, the torque can be developed by applying pulses having small duration. The linearized transfer function of the stepper motor is expressed in (13). Thus, a controller can be designed such that its transfer function is s/G (s). By applying pulse input, the motor produces a torque impulse as output. It is fed to the mechanical system, which is mathematically represented in (13). The angular position response is shown in Fig. 5. The results presented in Fig. 5 considers impulse response without controller. The final value of gain 'G(s)' is considered as 1. In this respect, amplifier gain is chosen such that steady state value of gain becomes 1 for a particular of N. For example, by taking the numerator as 1.2 for fixed N as 1:5, the impulse response gives the steady-state value of 1. In the condition, the gain value of amplifier is calculated as 6. The faster responses are appeared in Fig. 5 for variable gear ratios, which are plotted from the transfer function 'G(s)' in (13).

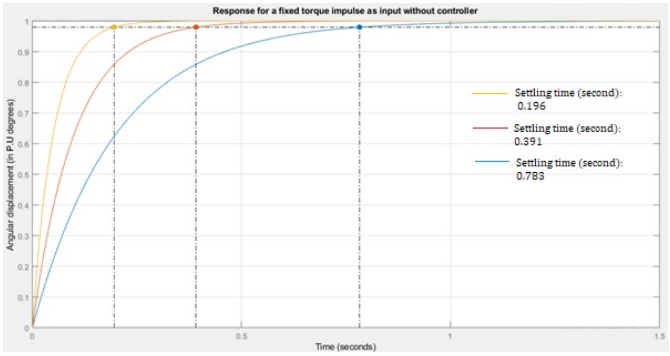

Figure 5. The angular position responses of gear system having variable gear ratios.

C. *Flowchart Representation of the Entire Proposed Process for Driving Tracking Motor and Arrangements for its Implementation*

The proposed process of aligning solar panel at optimum angle and subsequent dust removal activity is presented in three phases as marked in Fig. 6. In first phase of the process, all relevant inputs from environment are taken by the sensors and these are fed to the controller. There is a connector at the end of first phase of this flowchart, which leads to the second phase of the process. Here, in this phase, the slope is calculated by the formula given in (1). In the calculation of speed and direction, the wind sensor is used, which consists of a DC generator and small windmills (attached to the small DC generator). The output voltage from small DC generator is fed to the analog-to-digital converter (ADC), then the signal is fed to the controller. If the voltage from the wind sensor facing North is maximized, then wind direction is taken as North. If the difference between the output of two sensors facing two different directions is below a threshold value (very near to zero), then the direction is taken as either southeast or northwest. In next phase (second phase) of flowchart, the calculated slope of pressure vs. time in the previous phase is used and the controller checks whether the slope is less than or equal to -1mbar/second (the minus sign for decreased profile). If the condition is not satisfied (normal weather), then the process moves to the third phase. On the other hand, if the condition becomes true, storm is recognized. At this point, depending on the position of the panels i.e. let it be o with the horizon, the panel is rotated by (180-αo) through tracking motor. In effect, the front face of the panel faces the ground in first step as presented in Fig. 3. Then, depending on the obtained direction of the wind as discussed in just previous step, the panel is further rotated clockwise or anticlockwise by the motor to orient it at an optimum angle (-31°). Finally, after storm, the panels are cleaned by a clockwise and counterclockwise rotation of the axle after sand storm. In the logic under third phase of flowchart, if a storm approaches during the time of cleaning, then priority is given to prevent the erosion effects of the storm. Then, the dust cleaning process is restarted after storm. Finally, main steps of proposed methodology are sequentially summarized as:

- Detection of storm from estimation of rate of change of pressure,
- Finding of direction of wind,
- Orient solar panel at optimum angle by tracking motor-drive,
- After storm, cleaning of dust is done through repetitive jerking process by the motor-drive via its forward and backward rotational movement.

4. RESULTS AND DISCUSSIONS

A. *Detection of Storm and Subsequent Activation of Driving Motor for Making Reorientation of Solar Panel*

PSIM v 9.0 has been used for running the simulation. The simplified c block of PSIM has been utilized for simulating the pressure variation sensed by the pressure sensor and for the proposed wind sensors similar types of simplified c blocks have been used as shown in Fig. 7 and a stepper motor has been used. The simulation parameters are given in Table I

The components used for simulation are given in Table II. Simplified c blocks in the PSIM library are used to write logics of the flowchart of Fig. 6. The sampling rate calculation for the A/D converter is based on the work [5]. According to section 3 of this paper, whenever a dust storm occurs, it leads to a corresponding decrease in the

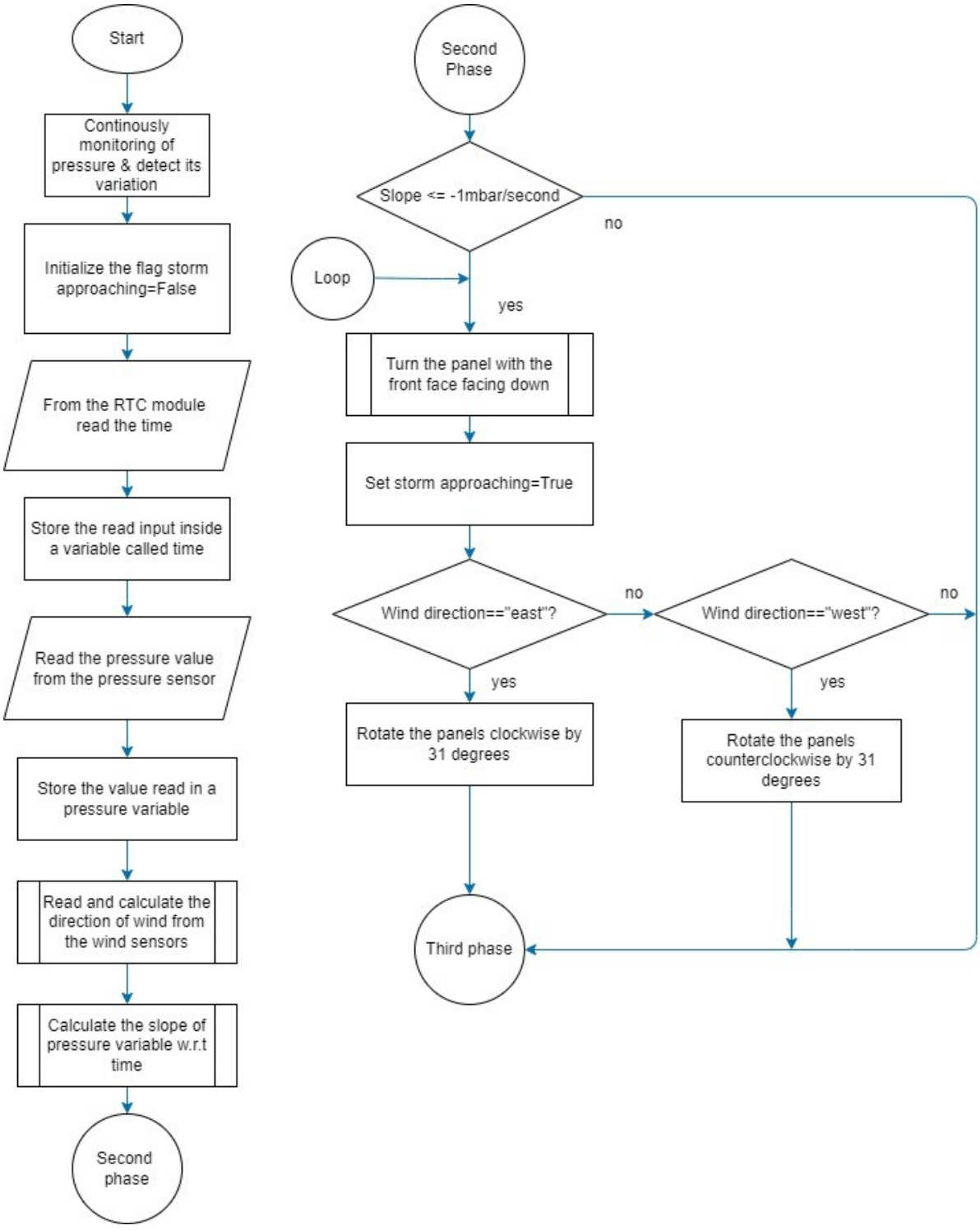
Start
Continously monitoring of pressure & detect its variation
Initialize the flag storm approaching=False
From the RTC module read the time
Store the read input inside a variable called time
Read the pressure value from the pressure sensor
Store the value read in a pressure variable
Read and calculate the direction of wind from the wind sensors
Calculate the slope of pressure variable w.r.t time
Second phase
Second Phase
Slope <= -1mbar/second
no
Loop
yes
Turn the panel with the front face facing down
Set storm approaching=True
Wind direction=="east"?
no
Wind direction=="west"?
no
yes
yes
Rotate the panels clockwise by 31 degrees
Rotate the panels counterclockwise by 31 degrees
Third phase

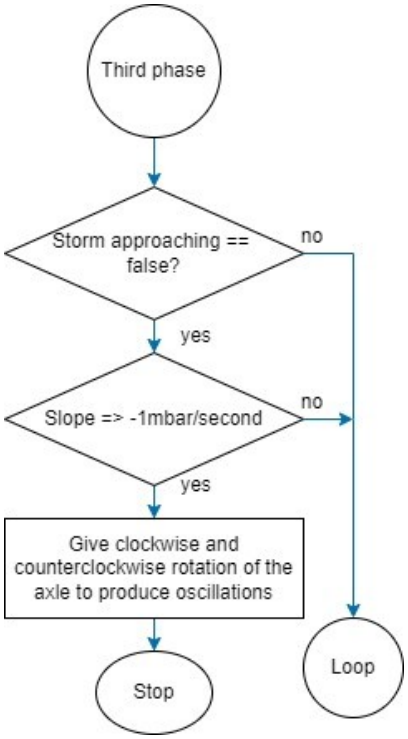

Figure 6. Flowchart showing steps of proposed logic in three phases.

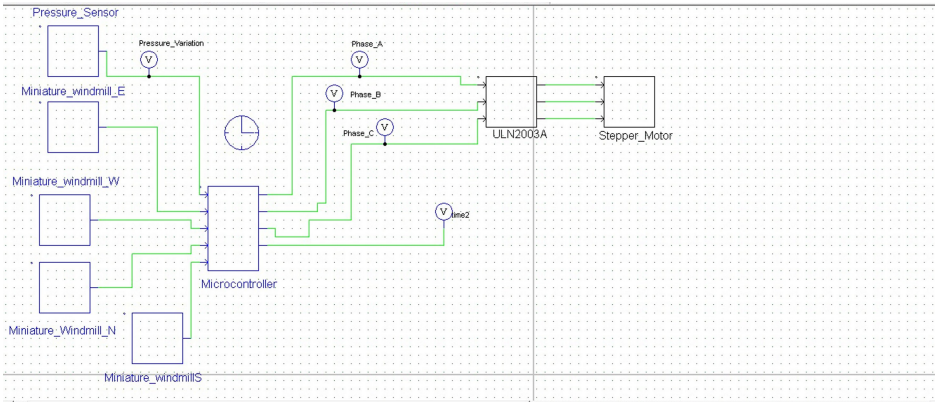

Figure 7. The PSIM model of proposed wind sensors-based motor-drive mechanism.

TABLE I. Simulation platform parameters

Simulation Parameter	Value (seconds)
Time step	10^{-5}
Total time	10
Print step	1

pressure. Regarding the calculation of sampling rate, the upper limit of the sand storm is taken as 150 storms/year and the lower limit is taken as 100 storms/year for the calculation of bandwidth as this range encloses the 95% confidence interval for the fitted curve by regression. Here, the resultant sampling rate is determined by the application of the Shannon's sampling theorem.

The pressure and wind sensors are realized using simplified C block in the PSIM model of Fig. 7 as stated before. In the simulation study, the hours have been mapped to seconds. The initial pressure is taken as 50 bars, which is given in Fig. 8. The output samples of pressure sensor are monitored by microcontroller block of Fig. 7. The logic written in this block checks rate of change of pressure (ROCOP) value whether it is equal or less than its threshold value (-1mb/sec). The microcontroller in the simulation model is programmed to trigger three pulses whenever the pressure drops below of 1mb in 1 second of simulation. In

first response of Fig. 8, before time (t) = 1 sec, it is observed that pressure drops linearly with a slope of -1mb/sec. Thus, storm is detected by the microcontroller block. It results generation of pulses by this block. The generated pulses (sequence of a-b-c) are given in Fig. 8. The pulses are applied to drive the motor via driver circuits as shown in Fig. 7. Here, if the algorithm written in microcontroller block detects a slope less than or equal to -1mbar/s, then the windings of the stepper motor are activated for orienting solar panel at before said optimum angle.

In the simulation study, pressure variation function is written in a simplified C block of PSIM library as given below,

```
y1=((-1*t+50)*(t<=1))+((1*t+50)*(t>=4))
```

Here, the pressure at the onset of storm decreases. This is modelled in the part ((-1*t+50)*(t<=1)). Then, for the duration up to 3 second, it remains low (Fig. 8). After this, the pressure again increases from 4th second onwards. The total simulation time is taken as 10 seconds. From (t) = 4 sec, pressure rises back to normal value. Now, the motor is rotated in the opposite direction to face the front of panel towards the sun (original position). Therefore, opposite sequences of three pulses (c-b-a) as shown in Fig. 8 are produced by the logic written in microcontroller block.

B. Study on Virtual Wind Flow Impact on Solar Panel

Now, a simulation study has been done to analyze the impact of blowing wind on solar panel in virtual wind tunnel using microCFD software. Here, the impact of sand/dust on the glass surface of a panel depends on the speed of the wind. Thus, the wind speed plays a vital role in determining the erosion rate of sandstorm in the panel [18] and if streamlines become parallel to the surface of the panel with reduced speed then less impact is achieved. In the study, Hyundai HiD-S300RGBK solar panel's dimensions have been used. The original length of the panel is 1675 mm, the width of the panel is 1001 mm and the depth of the panel is 33 mm. The solar panel is drawn using nanoCAD software. The drawing is shown in Fig. 9. Here, the scale factor is 1:5. Thus, the dimensions of solar panel in Fig. 9 is appearing as length of 335mm, width of 200.2 mm and depth of 6.6 mm. The nanoCAD model is required to use it in before said virtual study using microCFD software. In the virtual study, the wind speed of storm (scaled value of 1:5) is taken as 11.176 m/s. In a wind tunnel simulation, the Reynolds number needs to be conserved. In the study, the flow is subsonic. Therefore, for conserving the Reynolds number, the speed of the storm is taken as get 55.88 m/s (scaled value of 11.176m/s is multiplied by 5 to get actual value of 55.88 m/s). The corresponding Mach number [19] comes out to be 0.158 at the wind speed, and the temperature of the surrounding air is taken as 35 degree celsius. The software, which is used for simulation study, is micro CFD 2D virtual wind tunnel version 1.9 with a tunnel length of 2 meters. The height of the tunnel is 75% of its length i.e. 1.5m. Thus, the area of the wind tunnel comes out to be 3m2. All the parameter values that have been taken in the study are summarized in Table III. The computation of Reynolds number is available in the published literature [20]. This critical Reynolds number varies according to geometry [21]. The Reynolds number is calculated as follows,

$$Re = \rho u L/\mu \tag{13}$$

Where ρ is the density of the fluid, u is the flow speed and μ is the dynamic viscosity of the fluid. In MicroCFD software, a virtual wind tunnel [22] is used. It approximates the field by automatically generating meshes for the object under consideration by approximating the Navier-Stokes equation using initial and boundary conditions. In this scenario, blockage ratio plays an important factor. It determines required corrections, if any [23]. The blockage ratio is 0.01869 percent in the studied case, which is less than 3 percent and hence, no correction is required. The file is exported from nanoCAD in meters and the shapefile is edited. In the study, the direction of wind flow is taken from left to right and the velocity of sound in the air is 352 m/s.

TABLE II. Simulation components in PSIM platform (Fig. 7)

Sl. No	Component Name	Quantity	Specifications
1	Microcontroller (simplified C block)	1	The theoretical sampling rate of A/D converter for pressure sensing<= 315365.888 s/sample
2	Pressure sensor (simplified C block)	1	Sensitivity>= 1V/mbar
3	Wind speed sensor (simplified C block)	4	Sensitivity>= (2.5/11.76) Vs/m
4	ULN2003A stepper motor driver (simplified C block)	1	Nil
5	Stepper motor (simplified C block)	1	PminRated= 176.4W

Fig. 10 shows the velocity field near the boundary of solar panel in virtual wind tunnel simulation when the panel is oriented horizontally (0^o) with its downward face. In Fig. 10, the left-side legend shows the velocity of fluid flow in terms of Mach number. Its highest and lowest number is 0.189 and 0.019 respectively. The Fig. 10 shows that the speed of the wind near the panel varies from 39.761 m/s

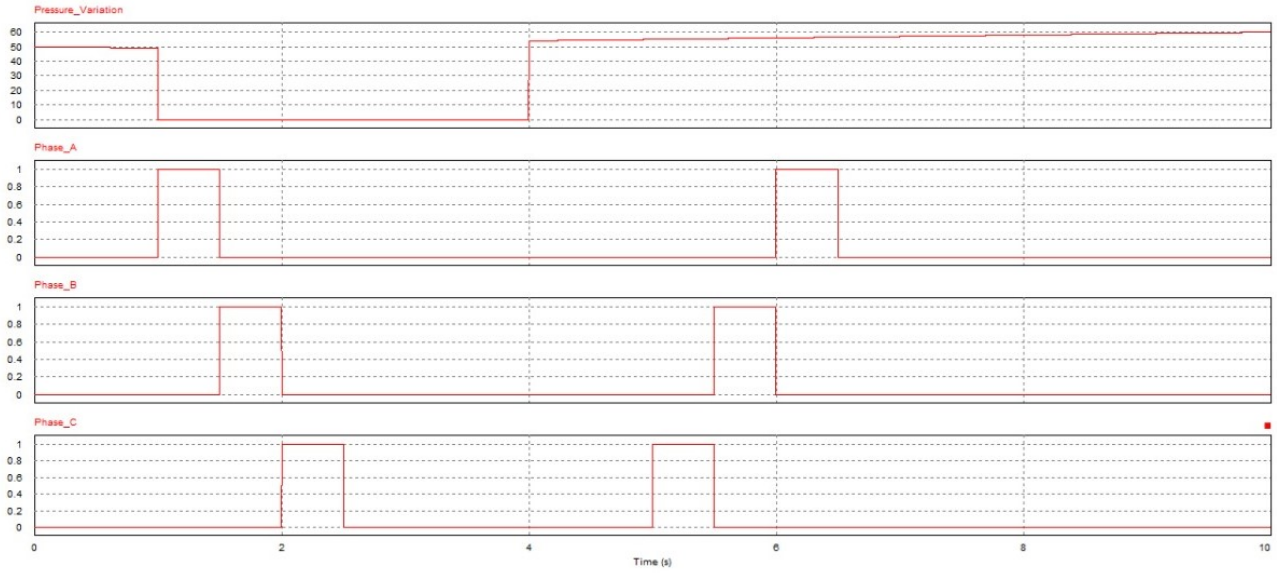

Figure 8. Pulse generation under the influence of pressure variation

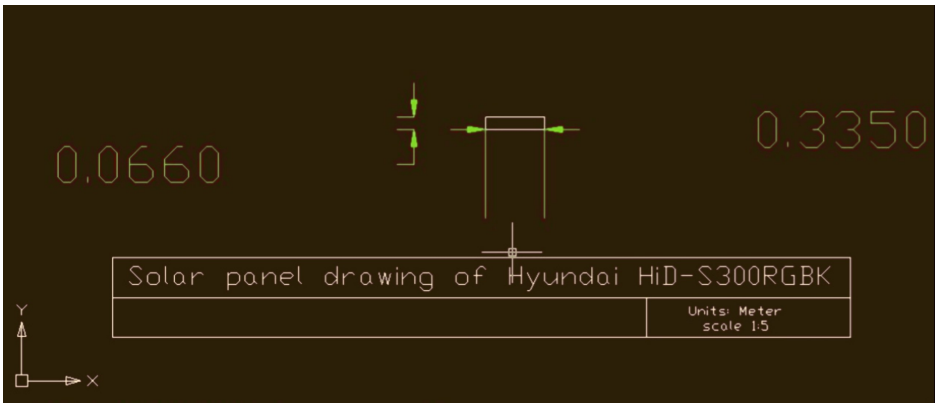

Figure 9. nanoCAD model of solar panel.

TABLE III. Simulation parameters for micro CFD

Parameter Name	Value
Length	2m
Width	1.5m
Mach number for the flow	0.158
The temperature of the air	35^oC
Scale	1:5
Model of the solar panel	Hyundai HiD -S300RGBK
Direction of flow	Left to right
Reynolds number	1131

to 46.464 m/s (7.9522 m/s to 9.2928 m/s with scale of 1:5 in Fig. 10). Thus, the speed of blowing wind during storm is reduced at near the panel from actual velocity of the storm (55.88 m/s). Further reduction of the air velocity near the panel is required. From further studies, minimum striking velocity is observed with -31^o tilting of the panel. The corresponding obtained velocity profile near the solar panel at -31^o is shown in Fig. 11. In the optimum angle, the velocity field near the front side of the panel is found in the range of 0 m/s to 8.096 m/s. Thus. the velocity field in Fig. 11 has been significantly improved to that of Fig. 10 i.e. striking velocity on the panel is significantly reduced at -31^o. The procedure for determining optimum angle (-31^o) will be provided in later validations and discussions. It can be mentioned here that the erosion rate is directly proportional to wind velocity. So, reduction of velocity lessens the impact at the optimum tilted position. Moreover, the streamlines, which are parallel to the panel surface, can avoid direct contact with the panel surface in the optimum position. The streamline profiles for 0^o and -31^o tilt angles are presented in the upcoming discussions and results.

The result in Fig. 12 shows that the streamlines at 0^o tilt angle of the solar panel are parallel to the surface and hence,

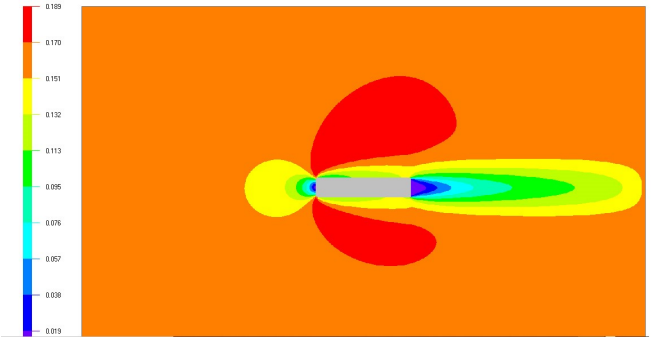

Figure 10. Velocity field near the boundary of panel at 0^o attack angle.

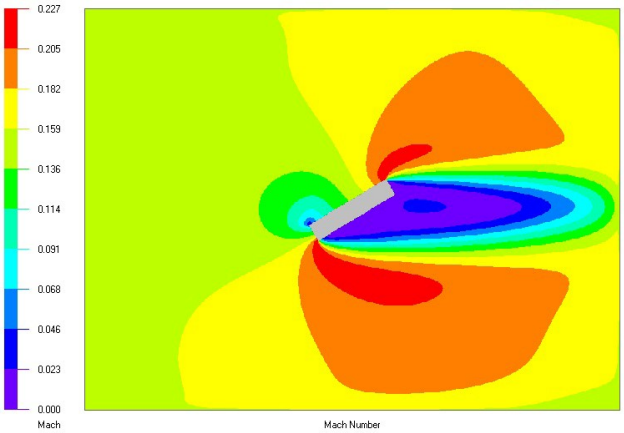

Figure 11. Velocity field near the boundary of panels at -31^o attack angle.

it reduces the deposition of dust. Regarding deposition of dust, Figgis, Guo and others [24] have specified that the deposition of coarse particles is fully controlled by gravity (sedimentation) in low wind-speed conditions. In windy conditions, turbulent eddies accelerate particles toward the surface, such that these may penetrate the viscous sub layer and impact the surface. Thus, this causes an inertial deposition rate in addition to the sedimentation rate. The streamlines for -31^o case are further improved as shown in Fig. 13. This reduces the impact on panel.

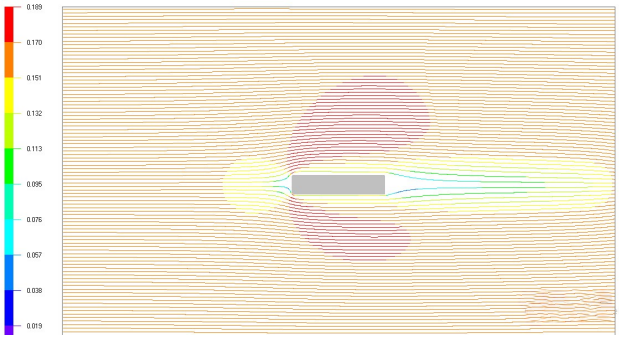

Figure 12. The streamlines around the panel oriented horizontally (0^o) with downward face.

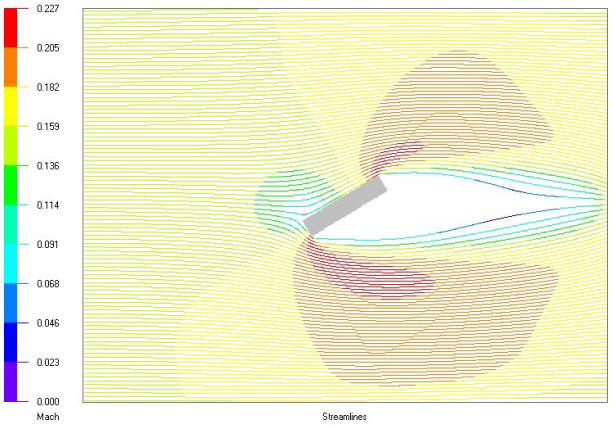

Figure 13. The streamlines along the surface of the panels at a -31^o attack angle.

The results of this exhaustive investigations are presented as follows:

C. CFD Simulation Results of Velocity Field for Different Striking Attack Angle

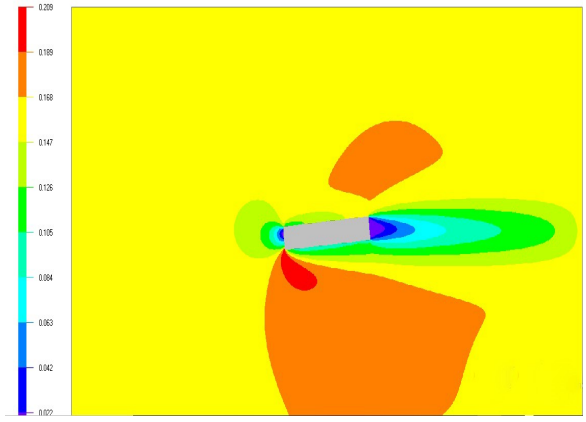

Figure 14. -5 degrees attack angle

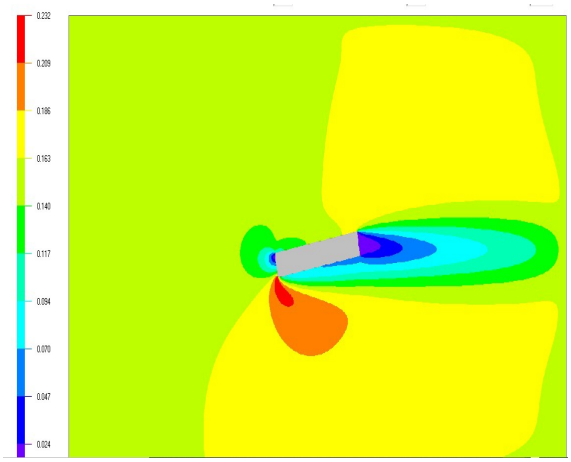

Figure 15. -10 degrees attack angle.

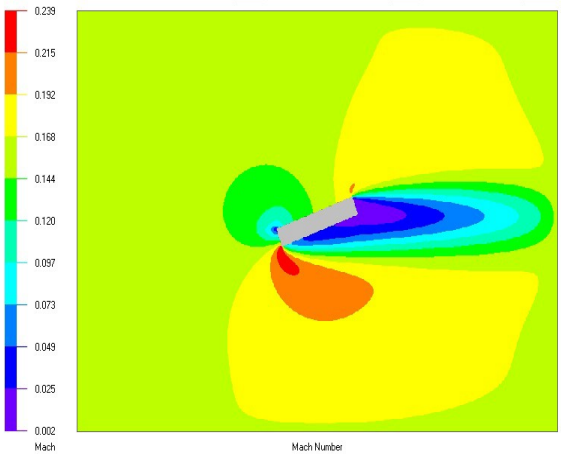

Figure 16. -20 degrees attack angle.

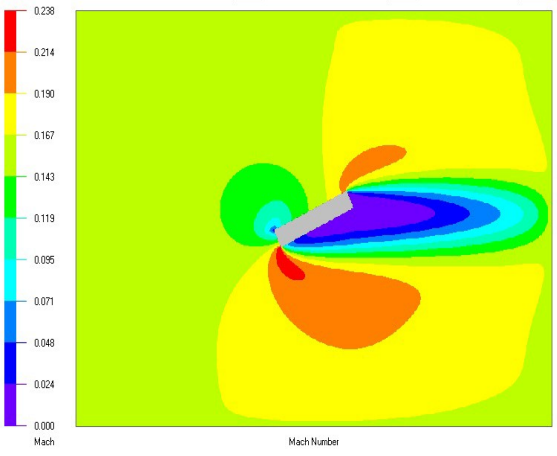

Figure 17. -25 degrees attack angle.

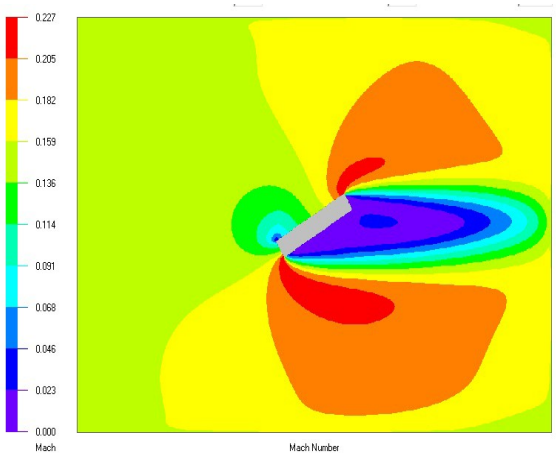

Figure 18. -30 degrees attack angle.

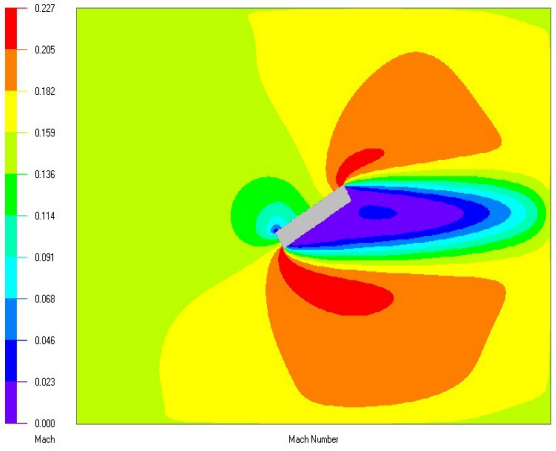

Figure 19. -31 degrees attack angle.

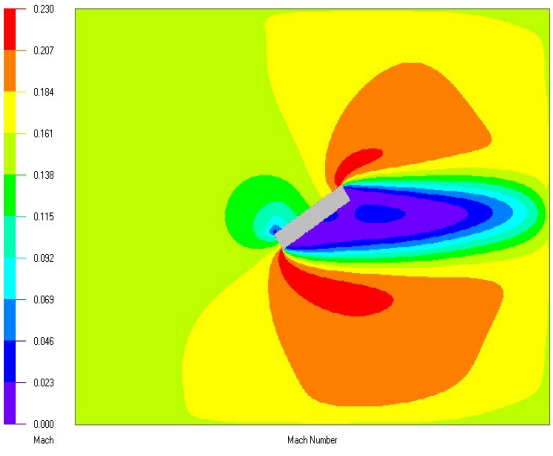

Figure 20. -32 degrees attack angle.

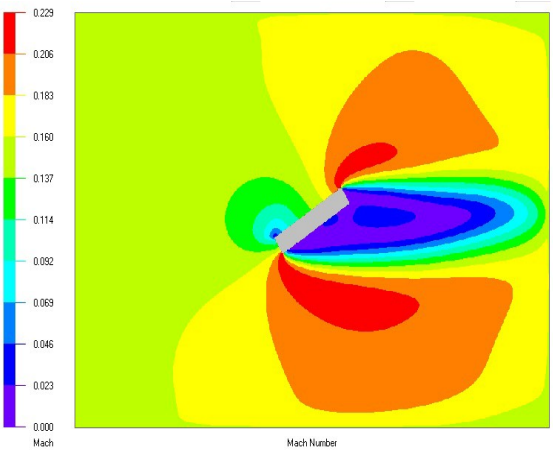

Figure 21. -33 degrees attack angle.

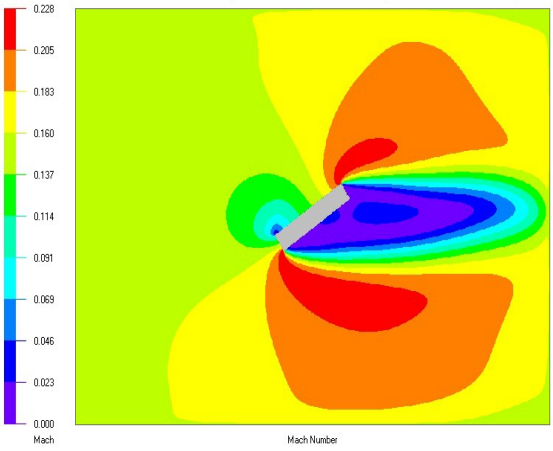

Figure 22. -34 degrees attack angle.

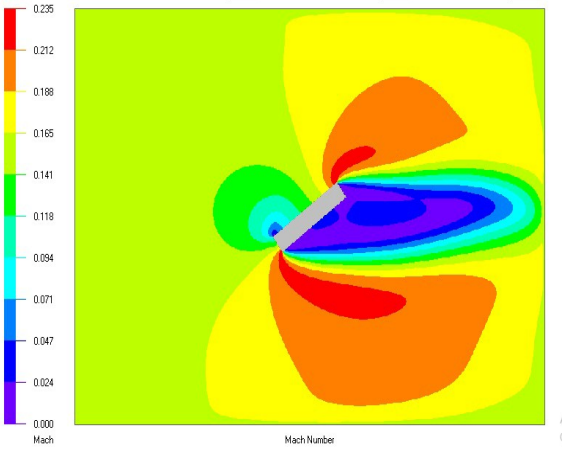

Figure 23. -36 degrees attack angle.

D. CFD Simulation Results of Streamlines corresponding to Different Striking Angle

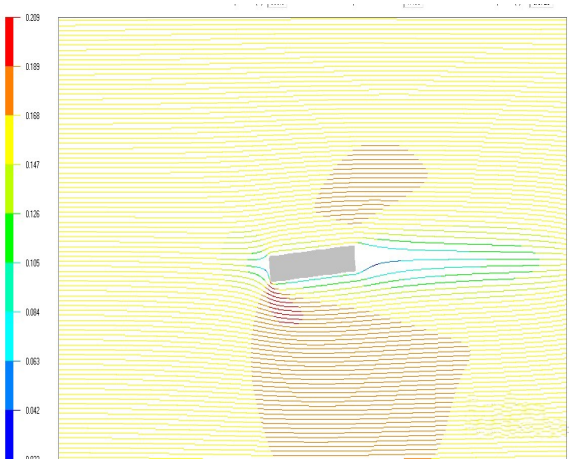

Figure 24. -5 degrees attack angle.

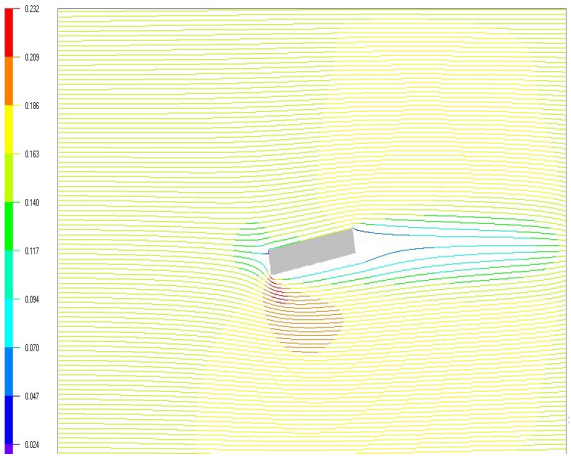

Figure 25. -10 degrees attack angle.

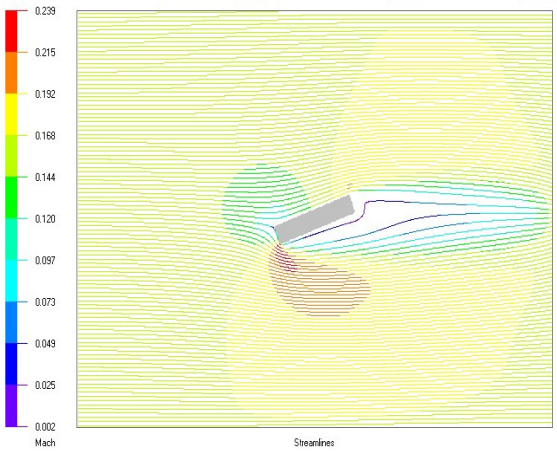

Figure 26. -20 degrees attack angle.

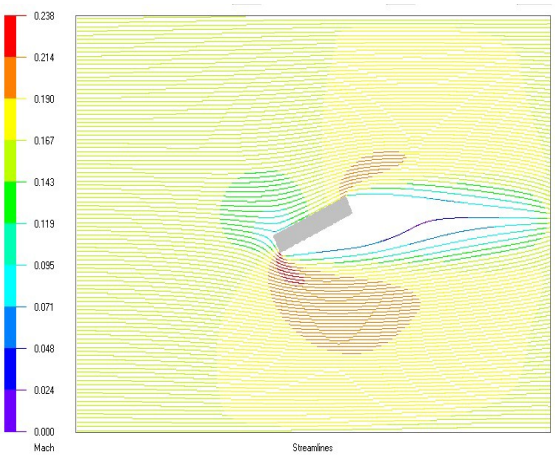

Figure 27. -25 degrees attack angle.

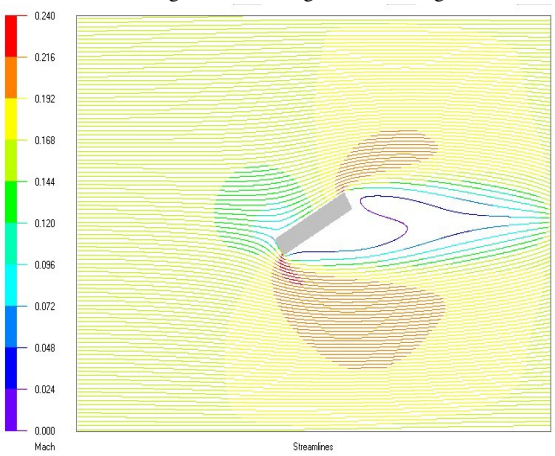

Figure 28. -30 degrees attack angle.

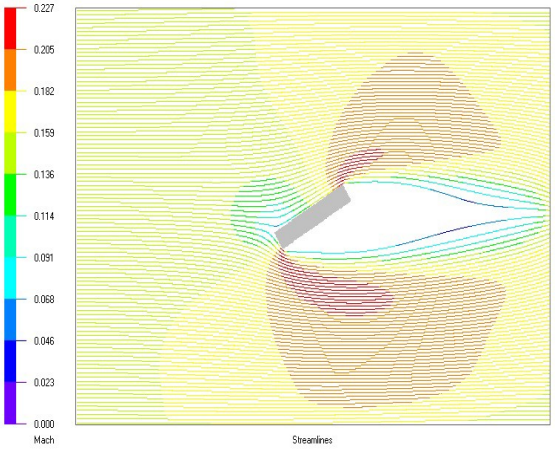

Figure 29. -31 degrees attack angle.

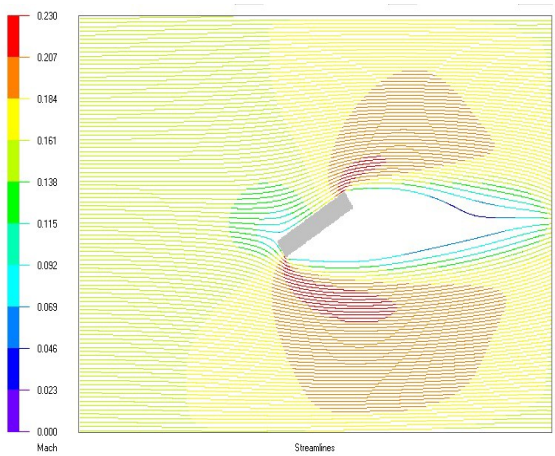

Figure 30. -32 degrees attack angle.

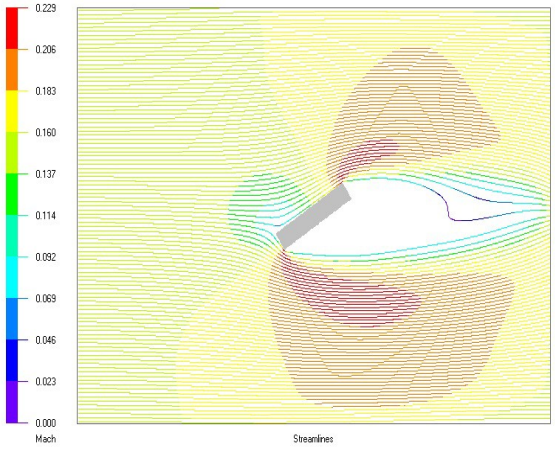

Figure 31. -33 degrees attack angle.

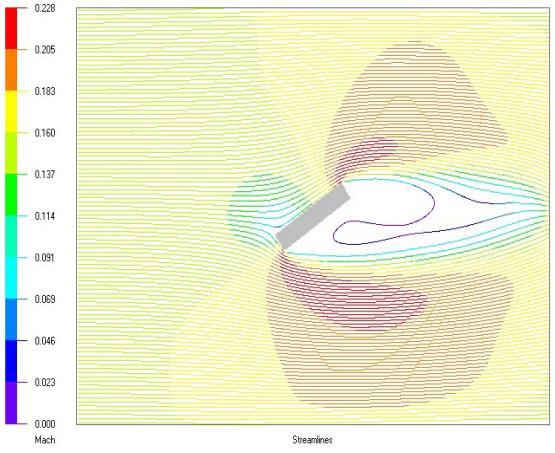

Figure 32. -34 degrees attack angle.

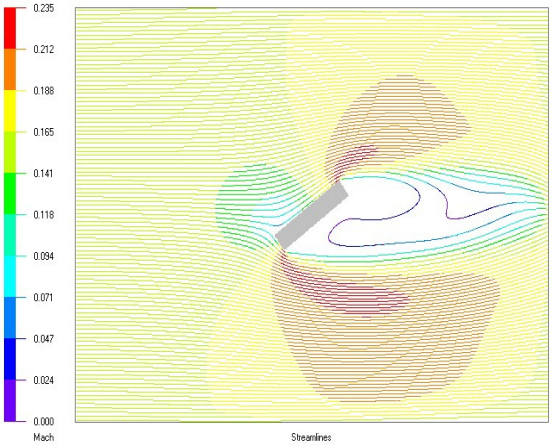

Figure 33. -36 degrees attack angle.

From Figs. 24 to 33, it is clear that the turbulence and its vortex appear near the boundary of the panel after 33^o of anticlockwise rotation of the panel. It may lead to the increased impact and dust deposition. On the other way, Figs. 14 to 23 show that the value of the velocity field starts to decrease in magnitude as the panel progressively rotates in the anticlockwise direction. Hence, there are two opposing phenomena i.e. decrement in velocity field magnitude and onset of turbulence with increasing value of attacking angle. In addition, further investigations are done in respect of lift and drag forces on solar panel. The lift and drag force will decrease stress of the structure over which the panel rests. In this study, various data are listed in Table IV. The data helps to find out optimum tilt angle of solar panel during storm. In this regard, following explanations are given:

The drag and lift forces depend on the square of the velocity. At -30^o, the wind velocity near the front part of the panel is slightly high in comparison to that of -31^o case. At -34^o, turbulence sets as given in Fig. 32. Hence, the optimal set of angles lies in the range of [-33^o, -31^o]. Now, in Table IV, -31^o is regarded as the optimum angle since the velocity near the front part of the panel is close to '0' as well as the resultant force is minimum at -31^o in the range of [-33^o, -31^o]. In case of -31^o, the resultant of lift and drag force is 34.53N i.e. lowest in the range. Therefore, -31^o is regarded as best position in the angle range.

The steps for deciding optimum angle are mentioned as,

- Investigations on velocity fields at different angles,
- Investigations on wind streamlines at different angles,
- Determination of angle range on the basis of low value of striking velocity and turbulence free streamline profiles,
- Calculation of resultant force on solar panel in the angle range,
- Determination of optimum tilt angle (-31^o) from the range in consideration of minimum force.

E. Structural Stress Evaluation for the Selected Optimum Angle

Structural analysis is very much important for sustainability of the construction under stress condition [25]. Here, the force applied to the top node is calculated using the data of Table IV. From the 9th row of Table IV, the lift force is obtained as 26.304 N/m in the downward direction. Since the length of the panel is 1.675m, the net downward lift force acting on the panel equals to 44.0592 N. But, additional 18 N of downward force is acting and hence, overall net downward force is calculated as 62.0592 N. Since there are three (3) panels in the study as presented in Fig. 34, the net force neglecting the weight of the axle comes out to be 186.177 N. This force gets divided into two king post trusses. Thus, individual lift force on the post truss is 93.088 N.

The drag force, according to 9th row of Table IV is 22.375 N/m. The length of the panel is 1.675m as given in Fig. 34. Hence, the net drag force is 37.478 N. According to Fig. 34, three panels are taken and thus, net force is 112.43 N. This force is equally shared by two trusses i.e. drag force on each truss is 56.217 N. The diameter of a section of the truss is taken as 12mm. The element is chosen as 304 types stainless steel having a young's modulus of elasticity as 200 GPa and the weight per unit length is 7850 Kg/m3. The results of Fig. 35 show that the maximum stress on the structure is 0.6906 MPa. Hence, the structure would remain intact as the ultimate tensile strength of stainless steel is around of 505 MPa [26]. Now, the second phenomenon that influences the process is cyclic loading. In this regard, the S-N curve is needed to be analysed for 304 types of stainless steel (Eagle National Steel, n.d.). In a year, this cyclic loading occurs 125 times. For 105 cycles of cyclic loading, the corresponding cyclic stress for failure is about 200MPa. Thus, the obtained results clearly indicate that the structure can tolerate far more cycles of stress than it receives in practice. The endurance limit of 304 austenitic stainless steel is 200MPa which is far more than 0.6906 MPa and hence, it is appearing from this discussion that no failure would occur. According to Goodman Soderberg's equation [27], the mean stress limit is 0.9996 MPa (endurance limit). In the study of this paper, the mean stress is obtained as 0.6906 MPa, which is below of the endurance limit. Thus, stainless steel structure of solar panel would remain intact for very long time in proposed method.

TABLE IV. List of CFD simulation results at different attack angles with scaling factor 1:5

Sl. No	Angle of attack (degree)	Parameters of simulation	Lift Force (Fl) and drag force (FD)	Velocity magnitude range near the front face of the panel that is facing down			
				Left (m/s)		Right (m/s)	
				Scaled Value	Actual Value	Scaled Value	Actual Value
1	0	Mach No: 0.158 Temperature: 308 K Tunnel length: 2m	Fl=2.5856 N/m FD=4.8104 N/m	7.9522 to 9.2928	39.761 to 46.464	7.9522 to 9.2928	39.761 to 46.464
2	-10	Mach No: 0.158 Temperature: 308K Tunnel length: 2m	Fl= - 18.2964 N/m FD=7.4808 N/m	4.928 to 6.6176	24.64 to 33.088	3.3088 to 4.928	16.544 to 24.64
3	-20	Mach No: 0.158 Temperature: 308K Tunnel length: 2m	Fl= - 27.8576N/m FD=15.10 N/m	6.8288 to 1.76	34.144 to 8.8	1.408 to 1.76	7.04 To 8.8
4	-30	Mach No: 0.158 Temperature: 308K Tunnel length: 2m	Fl= -28.85N/m FD= 22.1404 N/m	3.3792 to 1.6896	16.896 to 8.448	1.6896 to 0	8.448 to 0
5	-31	Mach No: 0.158 Temperature: 308K Tunnel length: 2m	Fl=-26.304N/m FD= 22.375N/m	1.6192 to 0	8.096 to 0	1.6192 to 0	8.096 to 0
6	-32	Mach No: 0.158 Temperature: 308K Tunnel length: 2m	Fl=-25.7848N/m FD= 23.5864N/m	1.6192 to 0	8.096 to 0	1.6192 to 0	8.096 to 0
7	-33	Mach No: 0.158 Temperature: 308K Tunnel length: 2m	Fl=-27.338N/m FD= 25.71N/m	1.6192 to 0	8.096 to 0	1.6192 to 0	8.096 to 0
8	-34	Mach No: 0.158 Temperature: 308K Tunnel length: 2m	Fl=-27.03N/m FD=25.768N/m	1.6192 to 0	8.096 to 0	1.6192 to 0	8.096 to 0
9	-36	Mach No: 0.158 Temperature: 308K Tunnel length: 2m	Fl= -26.8712N/m FD= 26.5192N/m	1.6896 to 0	8.448 to 0	1.6896 to 0	8.448 to 0

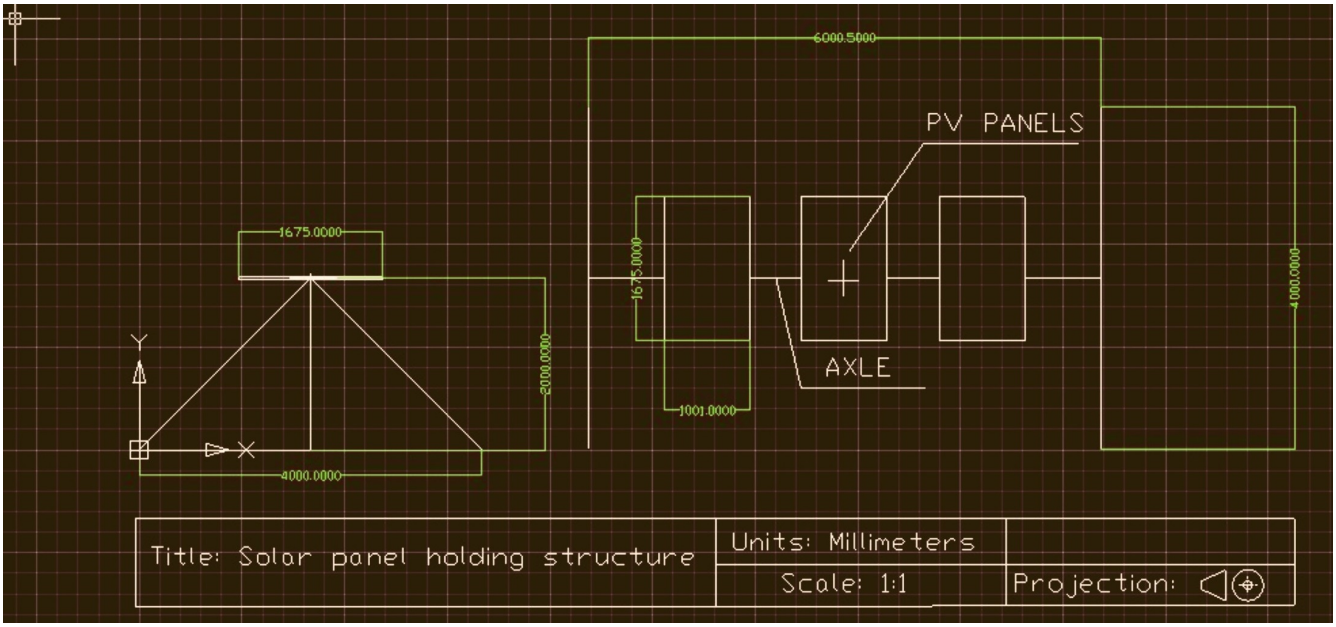

Figure 34. First angle projection of the structure holding the panels

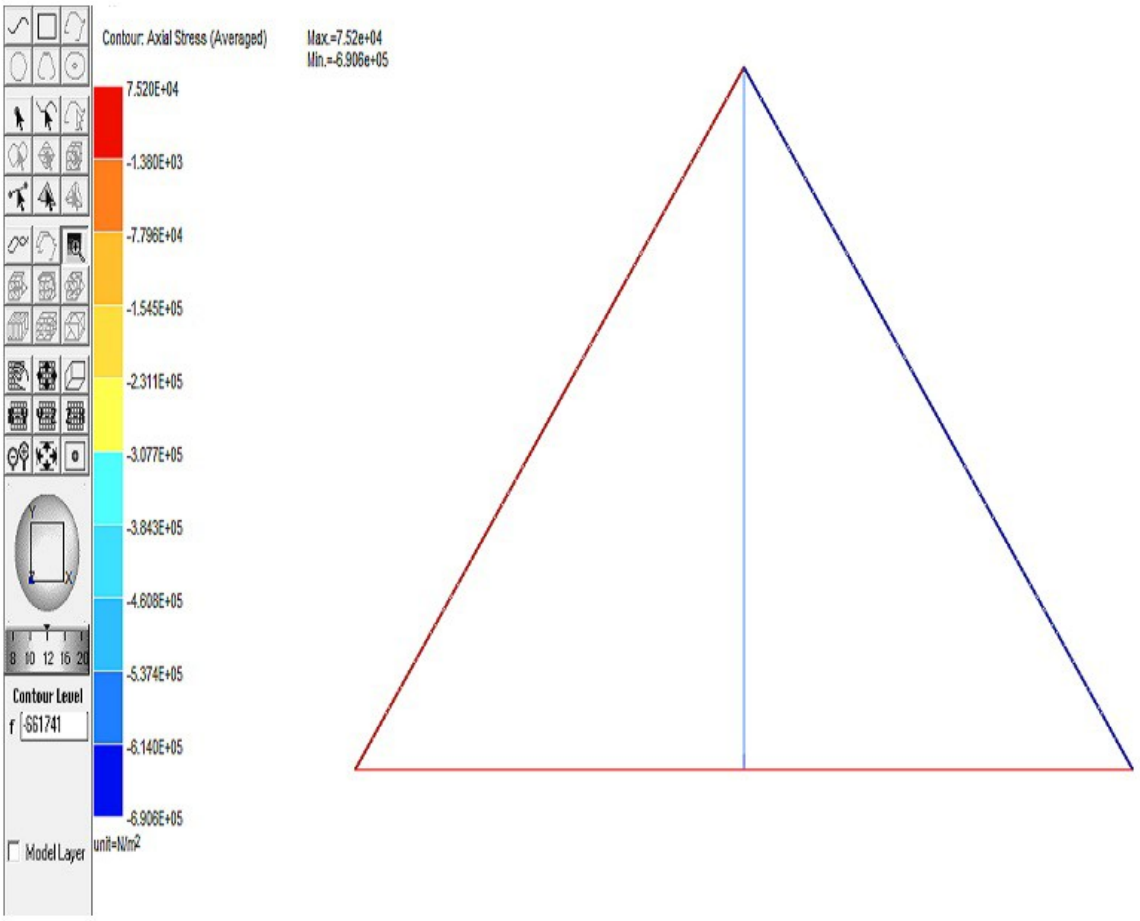

Figure 35. Stress contours corresponding to the lift and drag force developed by the solar panels on the supporting structure.

F. Test Setup

The experiment platform for verification of proposed algorithms (forward and reverse rotations of motor, positioning at optimum tilt angle via motor) with help of microcontroller and tracking motor is shown in Fig. 36.

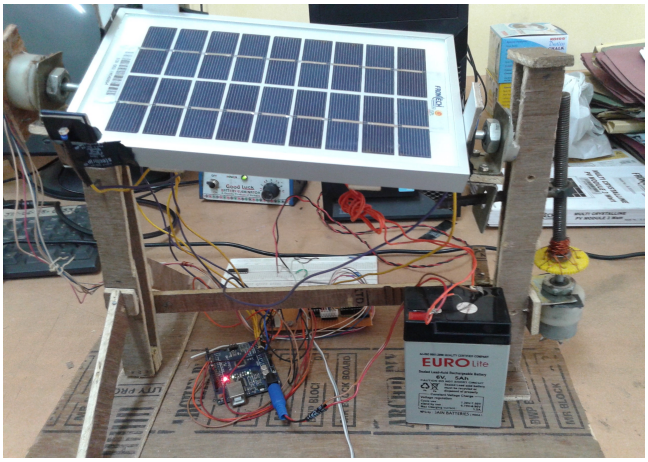

Figure 36. Test platform.

Here, the logical steps of flowchart in Fig. 6 are written using microcontroller (ATmega328p). This is used to drive the tracking motor having gearing arrangement through ULN2803 diver and other electronic circuits. The orientation at an angle of -31^o and forward and reverse rotations of motor are successfully achieved using the experimental setup. The responses are shown in Fig. 37. In upper sub-figure, the reference tilt angle (-31^o) is presented. The measured angle response attains the reference value. In lower sub-figure, repetitive 200 forward and return movement of motor drive is shown. Here, measured value tracks the reference angle value with reasonable accuracy.

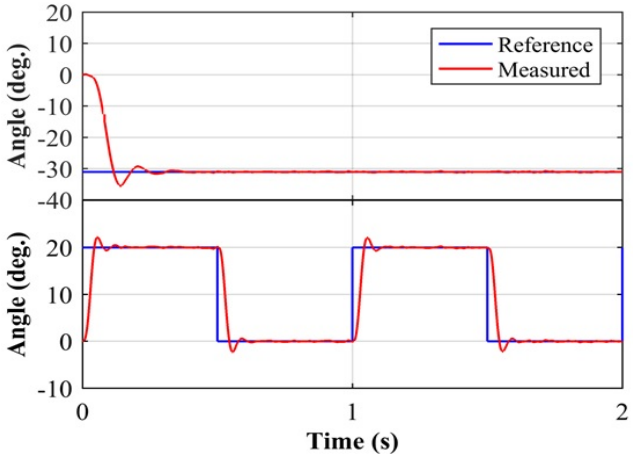

Figure 37. Position Angle responses in experimental study.

G. Performance Evaluation

The erosion rate (E) and degradation factor (DF) are computed as,

$$E = K.v \tag{14}$$

$$DF = E/E_n \tag{15}$$

In (14), 'K' indicates proportionality constant, which depends on type of erodent/particle [28] and environmental parameters. The 'En' in (15) indicates the nominal value of erosion rate at 10 m/s wind velocity. The comparative plots of 'DF' are shown in Fig. 38. In proposed case (-31^o), degradation due to erosion rate is less than 1 pu, whereas it is very high for conventional case (0^o with front face downward direction). These clearly indicate that the optimum tilt position significantly reduces the erosion and degradation process [29] of a solar panel during sand storm.

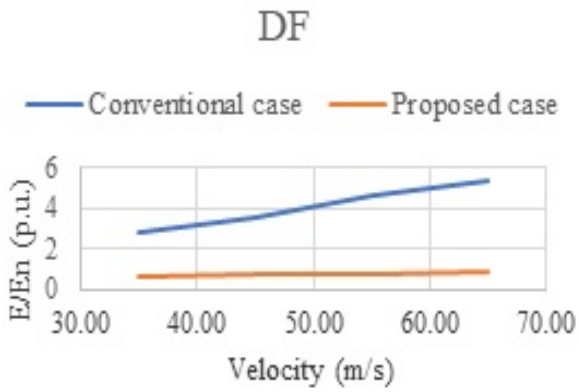

Figure 38. Comparative degradation factor.

The comparative features are given in Table V, which indicates proposed concept as better option.

TABLE V. Comparisons among various self-cleaning [30] schemes

Item	Method				
	Wiper along water	Nylon brush	Robot	Coating	Proposed
Dust cleaning	Yes	Yes	Yes	Yes	No
Reduction of attacking force by sand storm	No	No	No	No	Yes
Additional cost	Yes	Yes	Yes	Yes	No
Maintenance/Replacement	More	More	More	More	Less
Power requirement	Yes	Yes	Yes	No	Yes
Water requirement	Yes	No	No	No	No
Additional space/ infrastructure	Yes	Yes	Yes	No	No
Reliability	Medium	Medium	High	Medium	High
Durability	Medium	Medium	Long	Medium	Long

5. CONCLUSIONS

This paper proposes a new mechanism to avoid the impact of sand storm by using solar tracking motor-drive system. This also assists post storm cleaning process of solar panel in desert areas, which are heavily exposed to sand storms. The suggested cleaning method is cost-effective as it shares the motor-drive of solar tracker. Here, the clockwise and anti-clockwise angular movement of a solar panel is done by a stepper motor-drive system. Thus, it provides rapid clockwise and anti-clockwise transition of the panels and hence it assists the cleaning process for removing the accumulated dust due to sand storm. During sand storm, the proposed reorientation of solar panel increases the sustainability of solar panel and its supporting structure from erosion effect. In this regard, the impact of wind flow on solar panels and their structure is virtually analysed using CFD simulator. The simulation study on multiple orientations of the panel in the virtual 2D wind tunnel are performed and corresponding data is collected. Here, the reduction of the wind speed near the boundary of the panel and streamlines of the flow of dust parallel to the surface of the panel is noticed. From the virtual study, the optimum tilting angle of the panel is determined to minimize striking velocity on the panel. The optimum angle is found as -31^o along with the front face down during a sand storm. Here, the optimum angular orientation of the panel can be done by above mentioned motor-drive mechanism. In this connection, the erosion effect is mathematically analysed and significant reduction of sandstorm erosion is achieved at the optimum angle (it is reduced by 70-80% in comparison with conventional case). The stress on its supporting structure is also investigated from the tabulated lift and drag forces at the optimum position of solar panel and it is found that corresponding stress on the structure is 0.6906 MPa at above said optimum angular position, which is much below its ultimate stress. The proposed method is also compared with other state-of-arts to justify its superiority. Experimental validations of proposed algorithms are also done using a working prototype. The outcomes of the works are summarized as:

- Proposal of novel dust cleaning process
- Proposal of novel method to reduce striking force on solar panel by sand storm
- Determination of orientation of solar panel at optimum angle during storm via virtual study
- A cost-effective solution i.e. without additional infrastructures

ACKNOWLEDGMENT

The authors are thankful to Maulana Abul Kalam Azad University of Technology, West Bengal, India and Kalyani Government Engineering College, West Bengal, India and JIS College of Engineering, West Bengal, India for all kinds of supporting activity during the research works.

REFERENCES

[1] E. Kaplani, "Detection of degradation effects in field-aged c-si solar cells through ir thermography and digital image processing," *International Journal of Photoenergy*, vol. 2012, 2012.

[2] M. Abdelhamid, R. Singh, and M. Omar, "Review of microcrack detection techniques for silicon solar cells," *IEEE Journal of Photovoltaics*, vol. 4, no. 1, pp. 514–524, 2013.

[3] A. Rashki, N. J. Middleton, and A. S. Goudie, "Dust storms in iran–distribution, causes, frequencies and impacts," *Aeolian Research*, vol. 48, p. 100655, 2021.

[4] V. Gupta, M. Sharma, R. K. Pachauri, and K. D. Babu, "Comprehensive review on effect of dust on solar photovoltaic system and mitigation techniques," *Solar Energy*, vol. 191, pp. 596–622, 2019.

[5] S. Albugami, S. Palmer, J. Cinnamon, and J. Meersmans, "Spatial and temporal variations in the incidence of dust storms in saudi arabia revealed from in situ observations," *Geosciences*, vol. 9, no. 4, p. 162, 2019.

[6] N. M. Kumar, K. Sudhakar, M. Samykano, and S. Sukumaran, "Dust cleaning robots (dcr) for bipv and bapv solar power plants-a conceptual framework and research challenges," *Procedia Computer Science*, vol. 133, pp. 746–754, 2018.

[7] S. S. Wable, S. Ganiger *et al.*, "Design & manufacturing of solar panels cleaning system," *Int J Res Appl Sci Eng Technol (IJRASET)*, vol. 5, no. 07, pp. 191–197, 2017.

[8] A. Naik, N. Naik, and E. Vaz, "Abdulkareem,"automatic solar panel cleaning system"," *International Research Journal of Engineering and Technology (IRJET)*, vol. 6, no. 04, pp. 408–410, 2019.

[9] M. Burke, R. Greenough, D. Jensen, and E. Voss, "Project space: Solar panel automated cleaning environment," Santa Clara University 2016.

[10] B. M. M. Rathod Y U and J. M. S, "Automatic dust cleaning of solar panel with night sensing auto turn off mode," *Int. J. of Adv. Res. in Elec., Electron. and Instru. Eng*, vol. 07, no. 05, pp. 2711–2714, 2018.

[11] K. Ilse, M. Z. Khan, K. Lange, H. N. Gurumoorthy, V. Naumann, C. Hagendorf, and J. Bagdahn, "Rotational force test method for determination of particle adhesion—from a simplified model to realistic dusts," *Journal of Renewable and Sustainable Energy*, vol. 12, no. 4, p. 043503, 2020.

[12] C. Shi, B. Yu, D. Liu, Y. Wu, P. Li, G. Chen, and G. Wang, "Effect of high-velocity sand and dust on the performance of crystalline silicon photovoltaic modules," *Solar Energy*, vol. 206, pp. 390–395, 2020.

[13] D. Goossens, "The aeolian dust accumulation curve," *Earth Surface Processes and Landforms*, vol. 26, no. 11, pp. 1213–1219, 2001.

[14] B. Figgis, B. Guo, W. Javed, S. Ahzi, and Y. Rémond, "Dominant environmental parameters for dust deposition and resuspension in desert climates," *Aerosol Science and Technology*, vol. 52, no. 7, pp. 788–798, 2018.

[15] A. Al Shehri, B. Parrott, P. Carrasco, H. Al Saiari, and I. Taie, "Impact of dust deposition and brush-based dry cleaning on glass transmittance for pv modules applications," *Solar Energy*, vol. 135, pp. 317–324, 2016.

[16] K. Bryan, "Understanding inertia ratio and its effect on machine performance [white paper] retrieved november 25, from mitsubishi electric," 2019. [Online]. Available: https://us.mitsubishielectric.com/fa/en/support/technical-support/knowledge-base/getdocument/?docid=3E26SJWH3ZZR-41-13086

[17] H. K. C, "Applying the barometer to weather watching," 2012. [Online]. Available: http://www.islandnet.com/~see/weather/eyes/barometer3.htm(n.d.)

[18] D. Goossens and E. Van Kerschaever, "Aeolian dust deposition on photovoltaic solar cells: the effects of wind velocity and airborne dust concentration on cell performance," *Solar energy*, vol. 66, no. 4, pp. 277–289, 1999.

[19] M. G. Silva, V. O. Gamarra, and V. Koldaev, "Control of reynolds number in a high speed wind tunnel," *Journal of Aerospace Technology and Management*, vol. 1, pp. 69–77, 2009.

[20] K. Yousefi and A. Razeghi, "Determination of the critical reynolds number for flow over symmetric naca airfoils," in *2018 AIAA Aerospace Sciences Meeting*, 2018, p. 0818.

[21] T. A. Smyth, "A review of computational fluid dynamics (cfd) airflow modelling over aeolian landforms," *Aeolian research*, vol. 22, pp. 153–164, 2016.

[22] A. Gartmann, W. Fister, W. Schwanghart, and M. D. Müller, "Cfd modelling and validation of measured wind field data in a portable wind tunnel," *Aeolian Research*, vol. 3, no. 3, pp. 315–325, 2011.

[23] D. Sahini, "Wind tunnel blockage corrections: a computational study," Ph.D. dissertation, Texas Tech University, 2004.

[24] B. Figgis, B. Guo, W. Javed, S. Ahzi, and Y. Rémond, "Dominant environmental parameters for dust deposition and resuspension in desert climates," *Aerosol Science and Technology*, vol. 52, no. 7, pp. 788–798, 2018.

[25] Z. Moyan, X. Hong, M. M. Nadakatti, J. Feng, and L. Guangpeng, "Track structure failure caused by sand deposition: Simulation and experimentation," *Aeolian Research*, vol. 43, p. 100578, 2020.

[26] P. Strzelecki, A. Mazurkiewicz, J. Musiał, T. Tomaszewski, and M. Słomion, "Fatigue life for different stress concentration factors for stainless steel 1.4301," *Materials*, vol. 12, no. 22, p. 3677, 2019.

[27] "ch 12: fatigue. [e-book]desert (nasa earth observatory) retrieved 2 feb. 2021." [Online]. Available: https://earthobservatory.nasa.gov/biome/biodesert.php

[28] Z. A. Darwish, K. Sopian, and A. Fudholi, "Reduced output of photovoltaic modules due to different types of dust particles," *Journal of Cleaner Production*, vol. 280, p. 124317, 2021.

[29] F. Wiesinger, F. Sutter, A. Fernandez-Garcia, J. Wette, F. Wolfertstetter, N. Hanrieder, M. Schmücker, and R. Pitz-Paal, "Sandstorm erosion on solar reflectors: Highly realistic modeling of artificial aging tests based on advanced site assessment," *Applied Energy*, vol. 268, p. 114925, 2020.

[30] A. Al-Ahmed, F. A. Al-Sulaiman, F. Khan *et al.*, *The Effects of Dust and Heat on Photovoltaic Modules: Impacts and Solutions*. Springer, 2022.

Sudip Das Sudip Das was graduated in Electrical Engineering from Kalyani University in the year of 2004. After that he joined in Multi National Company as Asst. Engineer. He obtained his M.E (Power Engineering) degree from Jadavpur University in 2008. Now he is studying Ph.D in Electrical Engineering from MAKAUT. He is associated with JIS College of Engineering, Kalyani as Asst. Professor in Electrical Engineering Department since 2011. He has total six years industrial experiences more than eleven years in teaching experiences. He published twelve (12) numbers of International Journal nine (9) numbers of international conference. His research topic is implementation of renewable energy through Modern Automation Technology. He is also involving in research of smart water distribution system. He is a member of IEEE, Calcutta section.

Pritam Kumar Gayen Pritam Kumar Gayen is associated with Kalyani Government Engineering College, Kalyani, West Bengal, India as Assistant Professor in Electrical Engineering Department from 2010. He has published several papers on Grid Integration of Renewable Power Conversion System such as Solar and Wind Energy Conversion System, Power Electronics Drives, Power Quality, Nonconventional Energy.

Debamoy Datta Debamoy Datta is graduate scholar of Electrical Engineering from JIS College of Engineering, Kalyani.